Science of the Total Environment 906 (2024) 167713

Contents lists available at ScienceDirect

Science of the Total Environment

journal homepage: www.elsevier.com/locate/scitotenv

A ~5000 year multiproxy record of summer climate in NE Greenland

J. Garcia-Oteyza [a,*], S. Giralt [b], S. Pla-Rabes [c,f], D. Antoniades [d], M. Oliva [a], H. Ghanbari [d], R. Osorio-Serrano [b], D. Palacios [e]

[a] Department of Geography, Universitat de Barcelona, Catalonia, Spain
[b] Geosciences Barcelona (GEO3BCN-CSIC), Spain
[c] Universitat Autònoma de Barcelona, Bellaterra (Cerdanyola del Vallès), Catalonia, Spain
[d] Department of Geography & Centre for Northern Studies, Laval University, Quebec, Canada
[e] Department of Geography, Universidad Complutense de Madrid, Spain
[f] CREAF, Bellaterra (Cerdanyola del Vallès), Catalonia, Spain

HIGHLIGHTS

- Arctic lakes are climate change sentinels. Their sediments show natural climatic fluctuations and anthropogenic influences.
- High-resolution climate variability from NE Greenland based on lake sediments properties.
- Changing air temperatures were controlled by a mix of regional climatic changes and local landscape feedbacks.

GRAPHICAL ABSTRACT

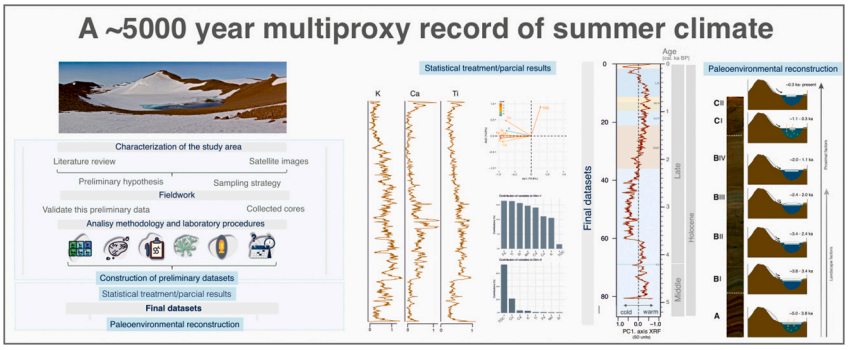

ARTICLE INFO

Guest Editor: Sergi González-Herrero

Keywords:
NE Greenland
Aucella Lake
Arctic lakes
Paleolimnology
Climate variability
Multiproxy analysis

ABSTRACT

The High Arctic plays a vital role in Earth's climate system, and its ecosystems are highly sensitive to global climate change. High Arctic lakes are valuable sentinels of climate change, as their sediments integrate long-term natural climatic fluctuations and anthropogenic influences. Here, we present a high-resolution ~5000 year-reconstruction of NE Greenland climate variability from Aucella Lake (74°N, 20°E) based on physical, chemical, and biological properties of lake sediments. We use CT-scans, hyperspectral imaging, organic matter, XRD, and diatom analyses to show that changing air temperatures were controlled by a mix of regional climatic changes and local landscape feedbacks. The latest Mid-Holocene (~5.0–3.8 cal. ka BP) was characterized by relatively warmer conditions, while the onset of the Late-Holocene was marked by abrupt temperature decreases that coincided with the beginning of glacial advances elsewhere (~3.8–3.4 cal. ka BP). From ~3.4–2.4 cal. ka BP, the sedimentary record indicated progressive warming, with temperature peaking during the Medieval Climate Anomaly, although temperature rises were punctuated by abrupt, short-lived cold periods. From ~1.1–0.05 cal. ka BP, the influence of landscape factors over the system diminished. Sedimentary indicators suggested a transition towards a colder, more humid climate, coinciding with the beginning of the Little Ice Age, that was characterized by a marked decrease in air temperature that reached minimum values at the end of this period.

* Corresponding author at: Department of Geography, Universitat de Barcelona, Montalegre 6-8, 3rd floor, 08001 Barcelona, Spain.
E-mail address: juliaoteyzaciria@gmail.com (J. Garcia-Oteyza).

https://doi.org/10.1016/j.scitotenv.2023.167713
Received 3 July 2023; Received in revised form 29 September 2023; Accepted 8 October 2023
Available online 10 October 2023

The last 50 years at Aucella Lake were marked by abrupt temperature rises, consistent with recently observed anthropogenic global warming. Our results illustrate the importance of high-resolution multiproxy studies for accurately characterizing lake linkages to their environment and climate.

1. Introduction

The High Arctic region is a crucial component of Earth's climate system, and its ecosystems are highly sensitive to global climate change (Anderson et al., 2017; Post et al., 2009; Saros et al., 2019). Both instrumental observations and future climate models reveal that the region is undergoing rapid warming, and it is expected to experience some of the most intense changes in response to climate warming by the end of the century (Preusser et al., 2008; Saros et al., 2019). According to >40 years of weather data, after 1994 CE mean June air temperatures increased by 2.2 °C in West Greenland and mean winter precipitation doubled from 21 to 40 mm, while since 2006 CE mean July air temperatures have increased by 1.1 °C (Saros et al., 2019). However, much remains to be understood about the drivers of Arctic amplification, climate variability and feedbacks (Lund et al., 2017; Pithan and Mauritsen, 2014; Serreze and Barry, 2011). Arctic climate change is non-uniform both spatially and temporally (Miller et al., 2010); to project future climate scenarios accurately it is therefore essential to contextualize present-day warming within a long-term perspective and thus decipher natural climatic fluctuations from anthropogenic influences. This is of paramount importance since the Greenland Ice Sheet may contribute between 5 and 33 cm to sea level rise by 2100 CE (Aschwanden et al., 2019). Furthermore, a detailed understanding of the short- and long-term temporal and spatial evolution of Greenland climate, mainly related to Greenland blocking, might help to provide insights describing the spatial and temporal evolution of the North Atlantic Oscillation (NAO), the major regional pattern of wintertime variability in the Northern Hemisphere (Davini et al., 2012; Hanna et al., 2016). According to some studies, an increasing trend of Greenland blocking in summer and a more variable blocking in winter may led to enhanced early winter NAO variability, mainly at the southern node of this climate mode (Hanna et al., 2015).

Lakes are considered to be sentinels of environmental changes as their physical, chemical, and biological properties respond rapidly to climate-related changes (Adrian et al., 2009; Catalan et al., 2013; Saros et al., 2019; Williamson et al., 2009). Lakes sensitively capture climate signals and environmental changes in the surrounding landscape and atmosphere (Goosse et al., 2018). Remote lakes, which are not directly influenced by anthropogenic factors (e.g. point sources of pollution, land-use changes and resource exploitation in their catchments), are often found at higher elevation and latitude and are among the most sensitive of such ecosystems (Carpenter et al., 2007; Pham et al., 2008; Williamson et al., 2008). Lake sediment properties offer continuous terrestrial paleoenvironmental archives that may be interpreted in the context of long-term climatic changes (Rosenzweig, 2007).

Although sediment sequences reconstructing local and regional Holocene climate have been published from several ice-free regions of Greenland, the spatial coverage is still incomplete, and temporal resolution is still coarse for many sites. Previous studies have shown spatial variation in Holocene temperature changes, and the timing of some critical events needs to be better constrained (Briner et al., 2016; Gajewski, 2015 and references therein). Moreover, most high Arctic Holocene climate reconstructions deal with temperature changes, and hydroclimate records should be a priority in order to reconcile ice sheet extension inferred from cosmic-ray exposure ages and geomorphological features with models of ice sheet evolution (McFarlin et al., 2018).

We sought to fill several of these knowledge gaps in a study of the remote Aucella Lake at 74° N, with the following objectives: (i) to refine our understanding of the timing and patterns of regional environmental and climate variability in NE Greenland; (ii) to produce a high-resolution geochemical, biological, and physical reconstruction from a remote lake on continuous permafrost terrain; and (iii) determine the climatic context driving glacial oscillations in the area. To achieve these goals, our specific objectives were to address the following questions:

- What was the natural climate variability in this area during the last several millennia?
- Were any observed climate oscillations synchronous with those recorded in other NE Greenland regions?

2. Study area

Aucella Lake (911 m a.s.l.; 74° 31.5044′ N, 20° 26.5231′ W), is a ~3.4 ha lake located near the top of the Aucellabjerg Mountain plateau (911 m), within the Wollaston Foreland peninsula in the SE corner of Northeast Greenland National Park (Fig. 1).

The lake's steeply sloped, glacial inherited catchment depression has an approximate area of 16.9 ha, and the lake has no defined inflowing streams. An NW outlet drains the lake, fed by a perennial snow patch of 0.06 km^2 area (Docherty et al., 2018) (on the north-facing slope), and descends through the Aucellabjerg slope forming the Aucellaelv stream, building an alluvial fan at the Zackenberg Valley bottom, and ultimately joining the main flow of the Zackenberg River. Geologically, while the Aucellabjerg Mountain slopes are composed of Cretaceous to Jurassic sedimentary rock units (mudstones, sandstones, and conglomerates) (Henriksen et al., 2009), the mountain plateau and the Aucella Lake catchment area expose Paleogene reddish-brown basalts (dominantly silica-oversaturated tholeiites) (Henriksen et al., 2009). The climate in this area is a polar tundra (Bonow and Japsen, 2021), with a mean annual air temperature (MAAT) recorded between 1996 CE and 2015 CE at Zackenberg Research Station weather station (situated at the valley bottom, at 700 m lower elevation) of −9.0 °C, and an average annual precipitation of 367 mm (Kottek et al., 2006) of which only 10 % falls as rain during the summer months (June to September) (Højlund Pedersen, 2017). Whereas the large lowland valley areas include moist to dry tundra dominated by shrubs with grasslands and fens (Hasholt et al., 2008), the variety and size of the plants decreases at higher elevations, with vegetation practically non-existent in the Aucella Lake catchment. The whole area is underlain by continuous permafrost with a thickness measured in the valley bottom ranging from 200 to 400 m and a spatially variable active layer that fluctuates between 45 and 80 cm thick (CAVM Team, 2003). The latest deglaciation studies in the area show that no glaciers have been present on the Zackenberg Valley bottom since the Early Holocene (ca. 10.5 ka; Garcia-Oteyza et al., 2022). However, cosmogenic surface exposure dating indicated that ice reached the landscape surrounding the lake during most of the last glacial cycle, arriving >800 m above the current valley floor during the maximum advance (ca. 80–50 ka) and probably also during the Last Glacial Maximum (Christiansen et al., 2010, 2008).

3. Methodology

3.1. Sediment coring

Fieldwork was carried out on July 26th, 2018. Sediment coring was carried out at the deepest known point (74° 31.3047′ N, 20°26.1528′ W) in the lake (~15 m) after using satellite images to establish target regions from catchment topography. One gravity core, AUC02 (83.6 cm) was recovered from the deepest part of the central basin (Fig. 1C), to avoid potential reworked sediment or sediment gravity flows from the margins, using a UWITEC gravity corer with a core diameter of 60 mm.

The water-sediment interface of both cores was immediately fixed using sodium polyacrylate (Tomkins et al., 2008); tubes were completely sealed at both ends and transported vertically in order to prevent disturbance and were then stored at +4 °C until they were opened for sampling in the laboratory.

3.2. Chronology

The chronological framework of the sedimentary sequence of Aucella Lake was constructed based on nine AMS radiocarbon dates exclusively measured on moss fragments, including a date of the core's surface in order to establish the presence/absence of a carbon reservoir effect in the lake. AMS radiocarbon samples were prepared at the Radiochronology laboratory of the Centre d'études nordiques, Laval University (Quebec City, Canada) and analyzed at the W. M. Keck Carbon Cycle Accelerator Mass Spectrometer Facility (Irvine, United States). The final age-depth model (see Section 4.1) was constructed Bayesian age-depth modeling in the R package rbacon (Blaauw and Andrés Christeny, 2011), with ages calibrated using the IntCal20 calibration curve (Reimer et al., 2020). In this study, our 0 cal. ka BP (or 'present') corresponds to 2018 CE.

3.3. Data and laboratory analysis

The sediment core (AUC02) was split lengthwise, with one half stored as an archive (in the cold room of the Geosciences Institute of Barcelona (GEO3BCN - CSIC) at +4 °C); the other half was used for non-destructive high-resolution analysis and subsampled at 1 cm resolution and stored in the same cold room until subsampling for destructive analysis.

3.3.1. Non-destructive analysis (CT-scan, XRF, hyperspectral imaging)

Before opening, all cores were scanned using a computerized 3D X-ray computed tomography Siemens Somatom 64 scanner (CT-scan) at the Institut National de la Recheche Scientifique, Centre Eau Terre Environnement (INRS-ETE) in Quebec City (Canada), to identify sedimentary structures (St-Onge et al., 2007). The sediment elemental composition (by X-Ray Fluorescence, XRF analysis) was then determined (Supplementary Fig. 1) using the ITRAX XRF Core Scanner at INRS-ETE with a resolution of 0.5 mm, a voltage of 1100 μA and a counting time of 10 s for eleven light elements (Al, Si, S, Cl, K, Ca, Ti, V, Cr, Mn, Fe) and seventeen heavy elements (Ni, Cu, Zn, Ga, Br, Rb, Sr, Y, Zr, Nd, Ba, Ce, Nd, Ta, Pb, Ra). The rest of the following analysis were performed only on the longest sediment core (AUC02). The cores were scanned using a hyperspectral scanner at the Aquatic Paleoecology Laboratory (LPA) in Laval University (Quebec City, Canada), equipped with visible-near infrared (VNIR) and shortwave infrared (SWIR) cameras (SPECIM, Oulu, Finland) covering the spectral ranges between 400 and 1000 nm and 1000–2500 nm, and having spatial resolutions of ~70 μm and ~180 μm, respectively. Hyperspectral images were used to infer high-resolution profiles of mean grain size distribution and total chlorophyll *a* (including degradation products) following the methodology established in Ghanbari and Antoniades (2022).

3.3.2. Destructive analyses (organic matter, XRD, diatoms)

Sediment samples were taken every centimetre for analysis of organic geochemical variables, including sediment organic matter (total organic carbon (TOC), total nitrogen (TN) and their stable isotopes ^{15}N

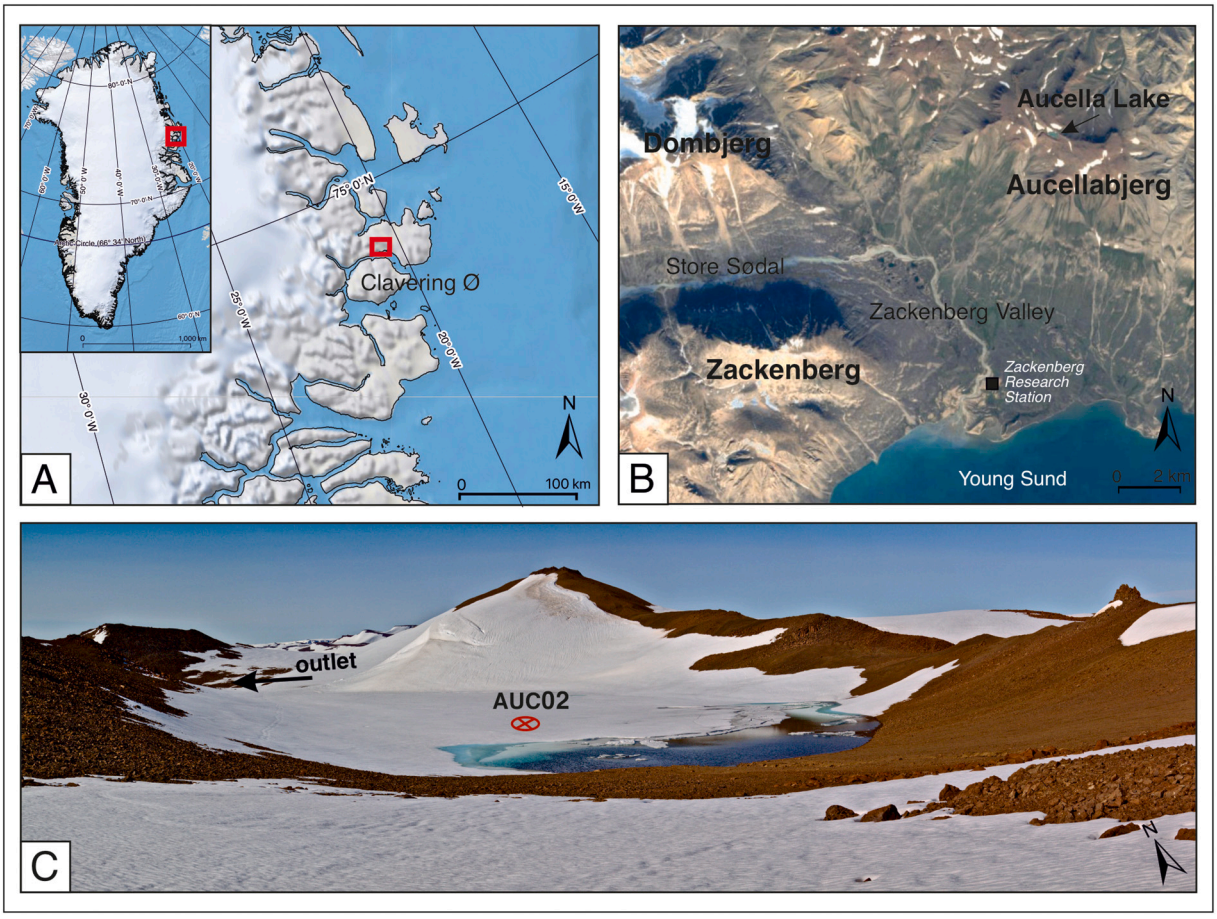

Fig. 1. Map of (A) study area within NE Greenland (B) Aucella Lake location in the Zackenberg area. (C) Picture of Aucella Lake with the location of AUC02 coring location.

and ^{13}C) as well as for mineralogical determinations. In both cases, samples were dried at 60 °C for 48 h and ground by hand using an agate mill. TOC, TN, $\delta^{13}C$ and $\delta^{15}N$ were determined using a Finnigan DELTAplus elemental analyzer-continuous flow-isotope ratio mass spectrometer (EA-CF-IRMS) at the Centres Científics i Tecnològics of the Universitat de Barcelona (CCiTUB). Mineralogy was determined by X-ray diffraction using a Bruker-AXS D5005 X-ray diffractometer in the following conditions: wavelength of 1.5405 A and ultrafast PSD detector between the angles of 4° and 60° 2theta, at GEO3BCN (Barcelona, Spain). Identification and quantification of the different mineralogical species present in the crystalline fraction were carried out following a standard procedure (Chung, 1974). 40 subsamples for diatom analysis were taken at ~2 cm intervals throughout the core. Diatom subsamples were processed with 33 % hydrogen peroxide (H_2O_2) and HCl (1 M) following the method described in Battarbee et al. (2001). At least 300 valves were counted at 1000× magnification with a light microscope and species are expressed as relative abundances (%) for each taxon. Taxonomic identifications mainly followed Krammer and Lange-Bertalot (1986, 1988, 1991a, 1991b), although basionyms were updated to follow current accepted nomenclature (https://www.algaebase.org/).

3.4. Data treatment

Statistical treatment of the datasets was performed in the R software environment v2022.12.0 + 353 (R Core Team, 2022), together with the packages 'rioja' (Juggins, 2022), 'vegan' (Oksanen et al., 2020) and 'factoextra' (Kassambara and Mundt, 2020). Only elements that had average values >300 cps in the XRF analyses were included, in order to ensure that the signal-to-noise ratio was high enough to characterize short- and long-term chemical variations with confidence (i.e., K, Ca, Ti, Mn, Fe, Cu and Sr). All variables were standardized and transformed prior to statistical analysis. Only diatom taxa representing >1 % of the total diatom sum were used in statistical analyses, and those with >4 % of the total diatom sum in at least one sample were plotted stratigraphically. Simpson's Index of diversity and principal component analysis of the Hellinger-transformed diatom relative abundance data were used to summarize the main trends in diatom assemblages (Legendre and Birks, 2012; Legendre and Gallagher, 2001). We also performed a stratigraphically constrained cluster analysis for each separate data group (XRF, XRD, mean grain size, organic geochemistry, chlorophyll, and diatoms) using constrained incremental sums of squares (CONISS; Grimm, 1987) (Supplementary Fig. 2).

We applied multivariate ordination methods to reduce the complexity of the large multi-proxy data set in order to identify underlying system dynamics, which required data pre-treatment. First, we averaged XRF data to the TOC resolution and carried out a PCA to reveal the relationships between the organic and inorganic sediment fractions. Second, we performed two redundancy analyses (RDA): one between the mineralogical composition of the sediments (explanatory variable) and the geochemical elements (response variable) to identify the possible provenances of the chemical elements; the second used the diatom assemblages as a response variable with the geochemical parameters as the environmental matrix (Supplementary Fig. 1A). To support (visual) identification of the main lithostratigraphic core units, we also conducted a constrained cluster analysis with measured datasets downsampled to 2-cm resolution and ran a broken stick model to identify the number of significant units.

4. Results

4.1. Age-depth model

Nine radiocarbon dates were determined from Aucella Lake sediments (Table 1).

Moss fragments in the surface layer of the sediment core returned an age of 1265 ± 20 cal a BP. The water-sediment interface was clear and sharp, with no indication of sediment loss or mixing, therefore, a deltaR value equal to the age of the core surface was applied to the rest of our radiocarbon ages. A slump between 42 and 45 cm core depth was identified from visual inspection and confirmed by two anomalously old radiocarbon ages that were excluded from model construction; this section of the core was also assumed to have been deposited concurrently for the purposes of the age-depth model. The sample at 44.5 cm was rejected as it represented a stratigraphic inversion. The age-depth model (Fig. 2) was thus constructed using a final dataset of six ^{14}C reservoir corrected ages using the Bacon R script and showed that the AUC02 core represents ~5000 years of sediment deposition, with limited variation in sedimentation rates throughout the core.

4.2. Lake stratigraphy and sediment characteristics

The core was divided into three main different lithological units (A, B, C). Zones inside unit B (BI, BII, BIII and BIV) and C (CI and CII) were established by visual identification (Figs. 3 and 4).

4.2.1. Unit A (83.6–68 cm depth) – age ~5.0–3.8 cal. ka BP

The sediments were mainly composed of centimetre-thick laminated light and dark brownish clays with macrofossils. Geochemically, there were peaks in several elements including K, Ca, and Ti in lowest part of the record, followed by a decrease and subsequent rise. Mn/Fe values remained high throughout the unit. Low values for grain size, and the dominance of clay minerals such as kaolinite, biotite/muscovite and, punctually, montmorillonite, highlighted the clay-rich nature of these sediments. In agreement with the visually evident macrofossils (mosses), organic indicators, including TOC, TN, and chlorophyll, had high values in this section (Fig. 4). Diatom assemblages were defined by the presence of *Staurosira venter*, followed by *Pseudostaurosira pseudoconstruens*, and other common taxa included *Staurosirella pinnata*, *Sellaphora seminulum*, *Sellaphora rectangularis*, *Rossithidium lineare* (although decreasing through the unit), and *Achnanthidium minutissimum* (Fig. 3). The transition to Unit B was clear both visually and in the CT-scan image, which had a sediment density boundary change from clay-rich to more sandy sediment.

Table 1
^{14}C dates of samples from the sediment core AUC02. Samples in italics were not included during the construction of the final age-depth model.

Sample ID	Midpoint (for age model, cm)	Dated Material	Lab Number	$\delta^{13}C$ (‰)	^{14}C age (BP)	±	Reservoir corrected ^{14}C yr BP
AUC 1802-0-1	0.5	Moss	UCIAMS-247345	−26.8	1265	20	
AUC 1802-11-12	11.5	Moss	UCIAMS-240752	−27.9	2425	15	1160 ± 25
AUC 1802-29-31	30.0	Moss	UCIAMS-240751	n/d	3255	15	1990 ± 29
AUC 1802-56-57	56.5	Moss	UCIAMS-240750	−26.4	4390	15	3125 ± 38
AUC 1802-70-71	70.5	Moss	UCIAMS-240744	−25.3	4820	20	3555 ± 38
AUC 1802–78	78.0	Moss	UCIAMS-221357	−25.2	5430	20	4165 ± 43
AUC 1802-42-43	42.5	Moss	UCIAMS-240753	−28.1	120	15	
AUC 1802-43-44	43.5	Moss	UCIAMS-261723	−28.1	Modern	2.1	
AUC 1802-44-45	44.5	Moss	UCIAMS-261724	−24.8	4460	15	

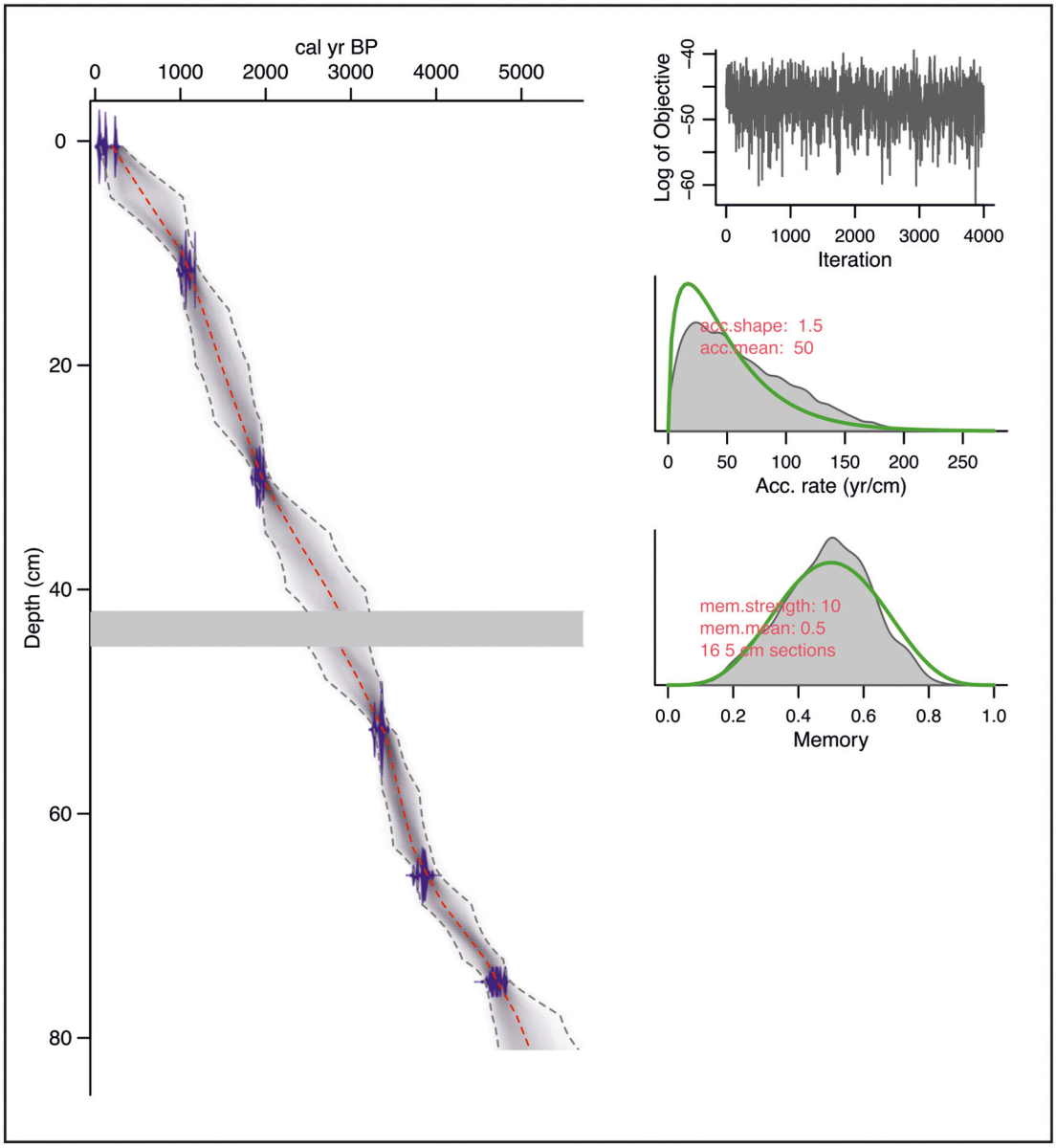

Fig. 2. Age-depth model for AUC02 based on bacon (Blaauw and Andrés Christeny, 2011). Right plot: shows the distribution of the radiocarbon dates in blue, assuming slump at 42–45 cm depth (grey rectangle). The age-depht model is shown in grey-scale, where darker hues indicate more certain areas. The red dashed curve shows the mean model and the dashed grey curves the 95 % confidence intervals. Left upper plot shows the MCMC (Markov Chain Monte Carlo) iterations of the run showing a stationary distribution with little structure among iterations. Left middle plot shows prior (green curve) and posterior (grey filled curve) distribution accumulation rates. The mean accumulation rate was 50 yr/cm. Left lower plot: shows the prior (green) and posterior (grey) probability distributions for the memory (i.e. autocorrelation strength).

4.2.2. Unit B (68–13 cm depth) – age ~3.8–1.1 cal. ka BP

Unit B's limits were marked by clusters in all proxy datasets, although the precise depths varied slightly. Overall, this unit was made up mainly of silty clays and sands in which four zones were distinguished:

4.2.2.1. Zone BI (68–59 cm depth) - age ~3.8–3.4 cal. ka BP. This zone's base started with sediment composed of well-laminated green/Gy silt. Geochemically, visible peaks were present in almost every element except for Sr, while Mn/Fe showed a slight decrease overall and less variability. The silty nature of the sediments was highlighted by a grain size increase, although with lower variability than in the previous unit, as well as by an abrupt change in the CT-scan. The organic parameters TN, TOC, and chlorophyll decreased markedly (Fig. 4). A peak of diatom diversity and richness appeared, and diatom assemblages in this zone were formed by increases in *Encyonema silesiacum* with the appearance of *Encyonema procerum*, *Adlafia* sp. B, *Amphora copulata* and *Naviculadicta* sp. A (Fig. 3).

4.2.2.2. Zone BII (59–39 cm depth) - age ~3.4–2.4 cal. ka BP. This zone was generally characterized by a massive brown silt sediment structure with macrofossils, although several centimetre-thick laminations were present at ~47 cm and ~41 cm core depth. A mass movement between 42 and 45 cm depth was identified based on visual evidence of perturbed sediment within a laminated unit, as well as by three anomalous radiocarbon ages within the zone (Table 1). As such, these 3 cm were removed from the record for the construction of the chronology as well as for paleoecological interpretations. All biogeochemical proxies showed trends in zone BII similar to those in BI. Mineralogically, zone BII was characterized by the presence of a montmorillonite peak and the

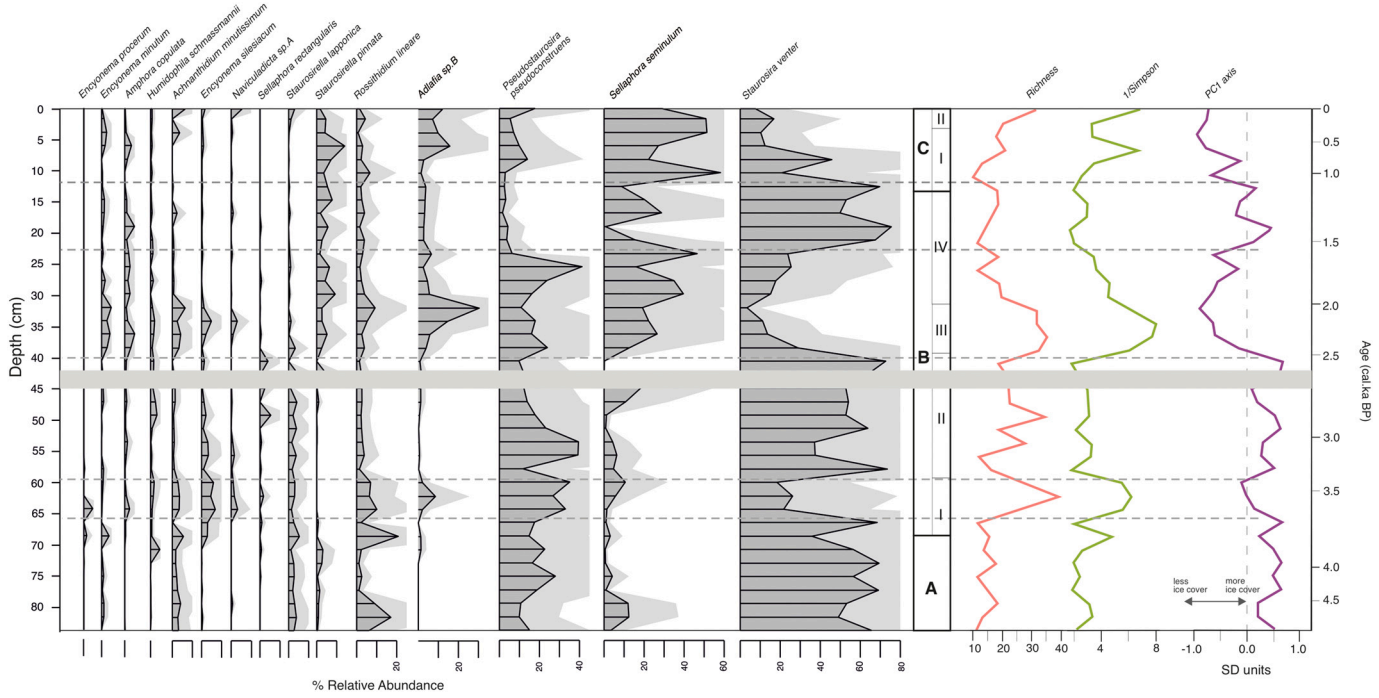

Fig. 3. Diagram of total diatom taxa valve abundance and (% total diatom valves) for AUC02 core; diatoms richness; Simpson's diversity index, sample scores on diatom PCA axis 1; diatom PC1 axis.

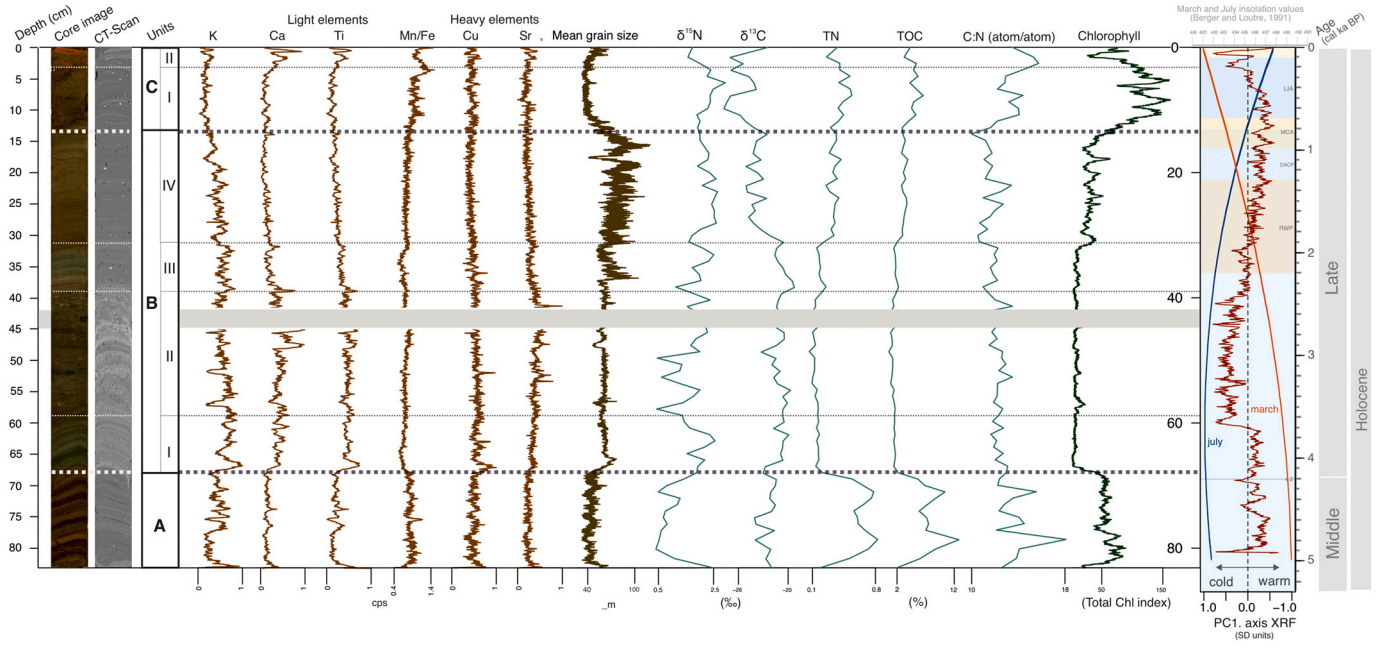

Fig. 4. Multi-proxy data from AUC02 sediment core. From left to right: depth scale; picture and Ct-scan image of the core; Physical characteristics: XRF; Grain size; Organic characteristics: C/N; Chlorophyll; XRF PC1 axis from Aucella Lake record (slump centimetres extracted); March and July insolation at 65°N (Berger and Loutre, 1991). Specific climatic periods/events are shown: Roman Warm Period (RWP), Dark Ages Cold Period (DACP), Medieval Climate Anomaly (MCA) and Little Ice Age (LIA), after Kolling et al. (2017).

highest values of kaolinite and plagioclase (Fig. 4). Diatom assemblages were strongly dominated by *Staurosirella lapponica*, *S. pinnata*, *Pseudostaurosira pseudoconstruens* and *Staurosira venter* (Fig. 3).

4.2.2.3. Zone BIII (39–31 cm depth) - age ~2.4–2.0 cal. ka BP. Sediments were millimetre-thick orange/greenish laminations. All elements showed a decreasing trend except K, which displayed values higher than the zone below. There was an abrupt increase in grain size upwards beginning at ca. 37 cm depth, followed by a gradual upwards decline. Organic matter indicators did not change significantly with respect to the zone below (Fig. 4). Diatom assemblages were diverse, with no clearly dominant taxa, a marked decline in the relative abundance of *Staurosira venter*, and a peak in the abundance of *Adlafia* sp. B (Fig. 3) and in Simpson's index.

4.2.2.4. Zone BIV (31 - 13 cm depth). - age ~2.0–1.1 cal. ka BP. This zone was composed of light and dark brown millimetre-thick silty clay laminations. Light element trend values decreased, with K doing so more markedly. In contrast, for Mn/Fe there is a slight increase on trend values and no major changes for the rest of heavy elements. Grain size increased gradually upwards in this section to ~15 cm depth and declined thereafter, although this trend was superimposed on significant variability, highlighting the unit's silty clay nature. Plagioclase, quartz, kaolinite, and biotite/muscovite displayed overall decreasing trends, while organic matter indicators and chlorophyll showed increased their values and variability with respect to unit BIII below (Fig. 4). Zone BIV was marked by the return to dominance of *Staurosira venter* and *Sellaphora seminulum*, as well as by the decrease of *Pseudostaurosira pseudoconstruens* and the disappearance of *Staurosirella lapponica* (Fig. 3).

4.2.3. Unit C (13–0 cm depth) - age ~1.1 cal. ka BP - present

4.2.3.1. Zone CI (13–3 cm depth) - age ~1.1–0.3 cal. ka BP. CT-scan results indicated that this zone was mainly composed of millimetre-thick laminae, although they were not visually evident and could be observed as brown clay sediment with macrofossils. Geochemical indicators did not display significant trends, apart from Mn/Fe values that increased upwards and had increased variability. Grain size decreased upwards in terms of both values and variability. The most significant peaks of montmorillonite appeared in this zone, along with the disappearance of nontronite and kaolinite and increases in the percentages of quartz and plagioclase. There was an increasing upward trend observed in TN, TOC, $\delta^{15}N$ and chlorophyll, and a decreasing trend for $\delta^{13}C$ (Fig. 4). Diatom assemblages were strongly dominated by *Sellaphora seminulum*, with declines in most other taxa except *Adlafia* sp. B and *Pseudostaurosira pseudoconstruens* (Fig. 3).

4.2.3.2. Zone CII (3–0 cm depth) - age ~0.3 cal. ka BP - present. This zone contained abrupt changes, with a visually notable decline in the quantity of macrofossils, and an orange hue in the upper centimetre. Elements including K, Ca, Ti, Cu, and Sr peaked in this zone, while Mn/Fe abruptly decreased. Mean grain size increased slightly, reflecting the silty clay nature of the sediments, and kaolinite reappeared along with a corresponding decrease in quartz. $\delta^{15}N$, TN, and TOC decreased, chlorophyll decreased abruptly, and $\delta^{13}C$ increased upwards to the sediment surface (Fig. 4). No large changes in the diatoms assemblages were recorded, only small increases in *Naviculadicta* sp. A, *Pseudostaurosira pseudoconstruens* and *Staurosirella lapponica*.

4.3. Multivariate analysis

4.3.1. Diatom assemblages

In terms of abundance, three diatom species dominated throughout the core and the main diatom zones were defined according to their shifts: *Staurosira venter* and *Sellaphora seminulum* and *Pseudostaurosira pseudoconstruens* (Fig. 3). The first two axes of the diatom PCA were significant according to the broken stick; the first explained 47.2 % and the second explained 18.2 % of the total variance. The three taxa with the strongest influence on the first axis were *Sellaphora seminulum*, *Staurosira venter* and *Adlafia* sp. B, while for the second axis they were *Pseudostaurosira pseudoconstruens*, *Staurosira venter* and *Sellaphora seminulum* (Fig. 5A). We focused our interpretations on PCA1 since it independently explained almost half the variance in the dataset.

4.3.2. Biogeochemical composition of the sediments

The first axis of the PCA of the XRF/organic matter data explained 73.6 % of the total variance (Fig. 5B) and was negatively associated with the lighter elements (i.e., Fe, Ti). The RDA of the XRF data with the mineralogical composition of the sediments as the constraining matrix showed the possible provenance of light and heavy elements obtained by the XRF. This RDA (Supplementary Fig. 1A) had one significant first axis that explained 87.8 % of the total variance. Ca, Ti, Fe, Mn, Sr, Cu, and K were mainly grouped with clays composed of moscovite/biotite, high $\delta^{13}C$ and kaolinite.

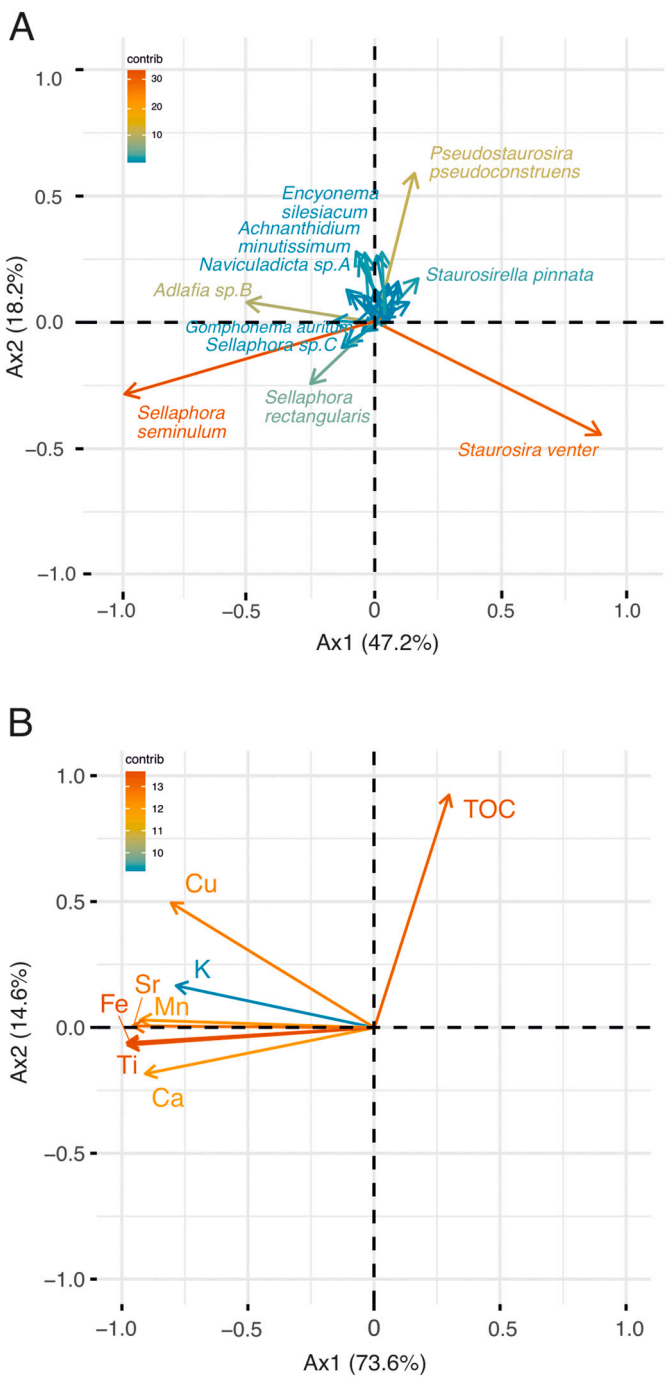

Fig. 5. Graphs (A) Diatom taxa PCA (B) XRF data combined with TOC PCA.

The first axis of the RDA constraining the diatom variance to the environmental dataset (Supplementary Fig. 1B) explained 34.8 % of the total variance and indicated that the three lower diatom clusters were associated with terrigenous inputs into the system and with an assemblage dominated by *Staurosirella* taxa. In contrast, the genus *Sellaphora* increased greatly in the three upper clusters of the record, where its interplay with *Staurosira venter* determined diatom zonation, and high abundance values of *Sellaphora* taxa were more strongly associated with high values of the internal ecosystem parameters such as $\delta^{15}N$.

5. Discussion

Interpretations of the PCA axes synthesize the local limnological and paleoenvironmental response to climate-related processes in Aucella Lake and its catchment. After understanding the baseline behavior of our ecosystem, we then compare our interpretations with other proxy data, both local and regional, and with globally known cold and warm periods, to compare local NE Greenland environmental change with that observed at larger scales.

5.1. Linking datasets: limnological processes

The first axis of the diatom PCA reflected climate-related processes (Fig. 5). Taxa associated with strongly ice-dominated polar lakes, including *Staurosira venter*, *Staurosirella pinnata*, *Staurosirella lapponica*, and *Pseudostaurosira pseudoconstruens* (Bouchard et al., 2004; Finkelstein and Gajewski, 2008; Kuhn et al., 1981), were strongly associated with the positive end of the axis. Conversely, the negative end was influenced by more diverse assemblages and epiphytic taxa such as *Sellaphora seminulum* (Emson et al., 2018), *Encyonema minutum* and *Amphora copulata* (Antoniades et al., 2008). The richness curve, which paralleled trends in PCA axis 1, further reinforced the dependence of this axis on climate, as longer ice-free seasons increase microhabitat diversity and therefore diatom diversity in high Arctic lakes (Smol, 1983). As such, the positive scores on the first diatom PCA axis represented cold water conditions with thicker and longer-lasting ice cover, while the negative scores were linked to longer ice-free summers that implied melting of the surrounding ice caps during wetter and/or warmer periods. The lack of planktonic diatoms in our sediments, similar to that observed in other Arctic lakes, may result from ice-free conditions that are too brief for their development, and/or from the high relief of the catchment preventing the wind-induced mixing of the lake required for diatom resuspension in the photic zone (Bouchard et al., 2004; Finkelstein and Gajewski, 2008; Paull et al., 2008).

The first diatom PCA axis divided the record into two clear sections (Fig. 2): the first (~5.0–2.4 cal. ka BP) showed positive values reflective of greater lake ice thickness and duration, and the second (~2.4 cal. ka BP – present) had predominantly negative values that indicated less severe ice conditions, albeit interspersed with some excursions towards more positive values. Richness and Simpson's index reinforced the linkages between diatom diversity and climatic changes, showing rises during periods of shorter ice cover duration shown by the first axis and the rise in water temperature of the Roman Warm Period (RWP) period. The sampling resolution of the diatom analyses (2-cm) implied an average interval of ~125 years, and these inferences therefore better capture long-term climate trends than high-frequency variations.

Sediment geochemistry was closely linked to catchment system dynamics, such as surface run-off during the ice-free season and ice cap melting periods, as confirmed by the RDA between the mineral species and the XRF, TOC and TN datasets (Supplementary Fig. 1A). Ca, Ti, Fe, Mn, and Sr were grouped mainly with clays derived from the catchment's primarily volcanic rocks, whereas the negative end of this axis was mainly triggered by changes in sediment biomass indicators TOC and TN. The absence of well-developed soils and vegetation around the lake and, therefore, of terrestrial organic matter in the basin, indicates that the majority of sediment organic matter was related to algal processes, a hypothesis also supported by the coincidence with low C/N ratios and $\delta^{13}C$ values. The association of montmorillonite with this negative end provides further evidence that lake primary productivity was associated with relatively warm conditions, since this clay is formed by the pedogenic alteration of pre-existent catchment rocks by hydrolysis under relatively warmer conditions (Fagel and Boës, 2008). The almost opposing trends of inorganic elements and lacustrine organic matter along the first RDA axis can be interpreted in terms of surface run-off. During relatively cold conditions, Aucella Lake may have remained partially ice-covered in summer, allowing the input of fine and non-chemically altered terrigenous particles from the catchment, whereas in relatively warm periods the lake was ice-free, permitting the input of previously formed soil clays into the lake as well as enhancing algal organic matter production. The thickness and duration of lake ice cover, as well as the amount of surface run-off in summer, are influenced by changes in air temperature (Sánchez-López et al., 2015). As such, variations along this first RDA axis reflect temperature changes. As the geochemical distribution in the RDA is almost the same in the PCA (almost opposing trends of inorganic elements and TOC) and the XRF data has better resolution than the RDA axis, the first axis of this is interpreted in terms of air temperature fluctuations.

The first XRF PCA axis (Fig. 4) shows a relatively warm period between ~5.0 and 3.8 cal. ka BP, during which ice cover was relatively thinner and/or less persistent and algal diversity was high, as shown by diatom diversity measures and PCA scores (Fig. 4). At 3.8 cal. ka BP, temperatures decreased abruptly, which coincided with the first decrease in algal diversity (Fig. 6A). Air and water temperatures remained relatively cold until ~3 cal. ka BP when air temperature started to gradually increase in consonance with the water temperature. Water temperature peaked at the onset of the RWP at ~2 cal. ka BP, while the air temperature peak occurred during the Medieval Climate Anomaly (MCA). The Little Ice Age (LIA) was marked by an abrupt air temperature decrease that reached minimum values at the end of this period. The Industrial Period was marked by a steep air temperature increase, thin ice lake covers and/or longer ice-free seasons, and a significant increase in diatom diversity.

The relationship between environmental factors in the RDA (Supplementary Fig. 2B) and the genus *Staurosirella* (a cold-tolerant and post-glacial pioneering taxon; (Smol, 1983) suggests its association with more turbulent environments, and with more movement or entry of material into the system. We hypothesize that the lower part of the core represented by the first three diatom clusters reflects a more turbulent or unstable environment dominated by more rapid changes, likely related to the dynamics of proximal factors such as the snow patch in the catchment area.

5.2. Local limnological and paleoenvironmental history

Other sediment core studies from the same area have documented changing conditions that were generally controlled by a mix of regional climatic changes and local landscape feedbacks (Bennike et al., 2008). Climate variability is regional (seasonal, inter-annual, and inter-decadal), while landscape factors, such as the behavior of the perennial snow patch inside the catchment area can be considered to be local (Hernández et al., 2015). Previous local studies suggested that this snow patch existed consistently in the uplands on Aucellabjerg Mountain from the early to mid-Holocene (Cable et al., 2018), which includes the early part of our sedimentary record, and that the winter snow patch size is an important driver of stream physico-chemical habitat in an Arctic region with low glacial cover (Docherty et al., 2018). Given that the sensitivity of the snow patch to changes in snowline elevation is primarily influenced by summertime temperatures (Oerlemans, 2001), the direct relationship between our temperature variation axis and the July insolation curve (Fig. 4) indicates that the evolution of Aucella Lake observed in our sediment core reflects summertime climate (Fig. 6).

Our air temperature record indicates that generally warm conditions prevailed during the mid-Holocene at Aucella Lake (~5.0–3.8 cal. ka BP) (Fig. 6, zone A). There were low, but present, inputs of terrigenous material to the system, showing that the lake became seasonally ice free during this period. Oxic conditions were present during the first thousand years of our record, with chlorophyll indicating high biomass, with at least the lake littoral zone thawing which allowed some nutrients to enter the system. Chlorophyll values suggest a lower snow accumulation above the lake ice cover and therefore dry conditions in the mid-Holocene. The input of newly formed clays, combined with high biomass variables, are related to higher rates of organic matter

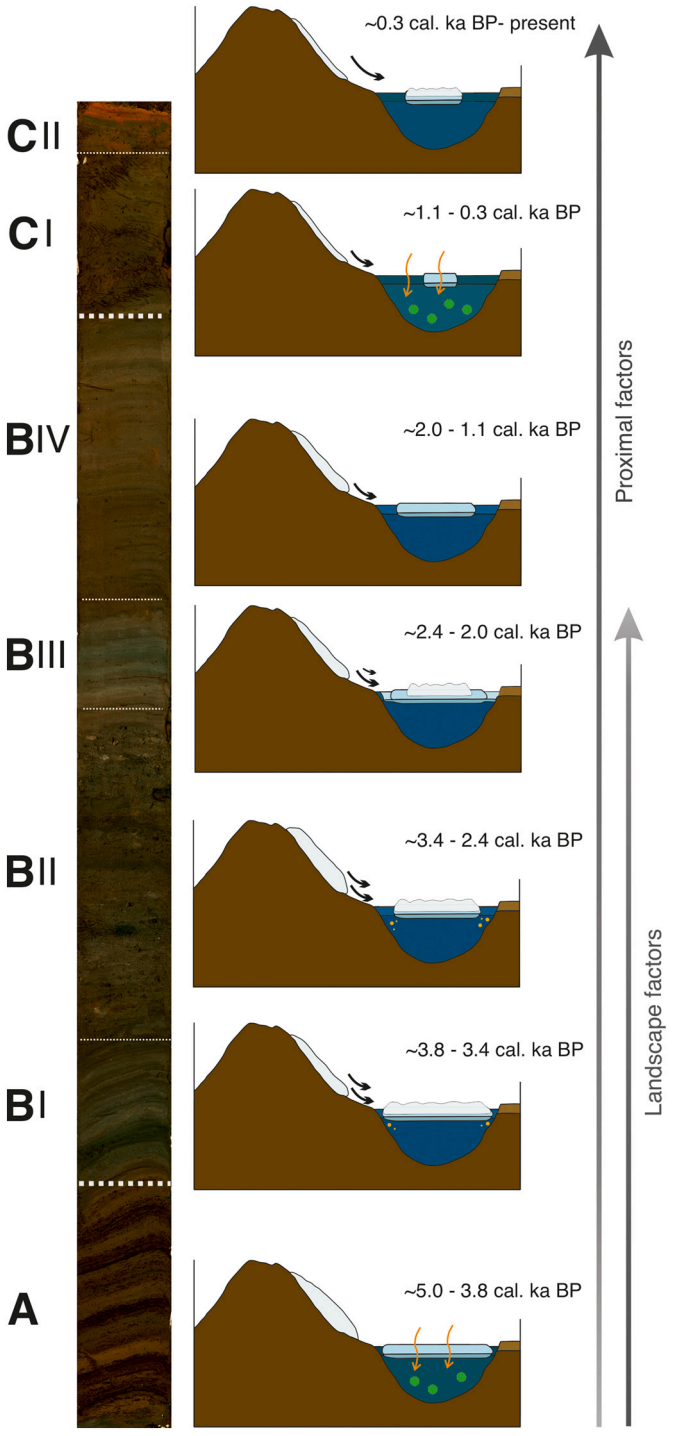

Fig. 6. Conceptual model of the of Aucella Lake evolution for each core zone.

productivity due to short periods of ice cover duration relative to other NE Greenland lakes (Smol, 1983). The rapid transition at ~3.8–3.4 cal. ka BP was the most abrupt in our record and was recorded by every proxies, although to a lesser extent by diatom assemblages. The abrupt change visible in terrigenous elements indicates enhanced delivery to lake sediments, and thus a more humid and colder climate that increased the transport of primary and non-chemically altered rock fragments from the catchment to the lake. Moreover, this increased input of terrigenous particles from around the lake increased turbidity and hindered light penetration, with a resulting decrease in diatom diversity and a longer ice-cover duration. During the next millennium (~3.4–2.4 cal. ka BP) (Fig. 6, zone BII), the sedimentary record was indicative of progressively warming conditions with high inputs of weathered terrigenous material, sustained by the continued domination of the snow patch as a landscape factor. Limited lake ice allowed high-continuous entry of material, as reflected by the fine grain size, and the continuity of low chlorophyll values suggests the presence of significant snow cover on the lake, in addition to high turbidity. Throughout the period ~2.4–2.0 cal. ka BP (Fig. 6, zone BIII), with the onset of the RWP, the diatom index and axis curves show (Fig. 2), on the one hand, a decrease of species diversity together with a significant change in the trend of PCA axis, on which more negative values show a shift to colder conditions with thicker and/or more persistent ice cover on the lake. This shift reflects a regime change that occurred in the system, when it ceased to be dominated by landscape factors (with large inputs of weathered terrigenous due to the activity of the snow patch) and began to record signals more dominated by regional climate variability. This is reinforced by an abrupt air temperature oscillation.

The sedimentary record then indicates a progressive transition to a warmer and drier climate at ~2.0–1.1 cal. ka BP (Fig. 6, zone BIV) peaking at the MCA. The highest temperatures coincided with a drop in grain size and terrigenous inputs, as well as an increase in chlorophyll values and the highest values of diatom diversity, suggesting longer ice-free periods during summer. Over the next several centuries, from ~1.1–0.3 cal. ka BP (Fig. 6, zone CI), the influence of landscape factors over the system diminished, and sedimentary indicators suggested a transition towards a colder, more humid climate that coincided with the LIA; air temperatures reached their minimum values at the end of this period. Diatom assemblages also had low diversities during this period, most likely linked to an increase in the duration and/or thickness of ice cover. An abrupt change was recorded during the last 50 years of the record (Fig. 6, zone CII), with increased diatom diversity and warmer conditions marked by thin ice covers and/or long seasonally ice-free periods, and an abrupt air temperature increase which almost reached the MCA peaks/relative trends. A parallel shift towards increasing mean grain size and high chlorophyll values imply rising temperatures and a potentially more turbulent environment that reflect recent warming as observed at high latitudes.

5.3. *Local to supra-regional inferences proxy correlations*

The closest multiproxy lake study to our site is located at the bottom of the Zackenberg Valley (at ca.8 km distance), and extends to 9.0 cal. ka BP (Bennike et al., 2008). The authors inferred an overall trend of declining summer temperatures and longer-lasting snow cover from 5.5 cal. ka BP to the present, unlike the trends we observed in Aucella Lake for the last 5.0 cal. ka BP. The Aucella Lake abrupt change recorded ~3.8 cal. ka BP was not observed in the Renland Ice Core oxygen isotope record (ca. 400 km south from Zackenberg), which may indicate that this abrupt shift was associated with landscape factors. The importance of local influences (size, depth, morphology and chemistry of the catchment) for the sedimentary record and lake biology has already been noted from NE Greenland sites (Bennike et al., 2008). A high-resolution record of proglacial Madsen Lake, ~20 km to the W, showed three phases of enhanced glacial activity during the last two millennia, with two phases between ~1.3–0.8 cal. ka BP and a third phase at ~0.7 cal. ka BP (Adamson et al., 2019). The Aucella Lake core records the onset of Late Holocene climatic deterioration at ~2.5 cal. ka BP, early for NE Greenland and preceding the Madsen Lake record, and also shows temperature minima coincident with the first two phases of glacial advance (~1.2 and ~0.8 cal. ka BP) recorded in this nearby study (Adamson et al., 2019). This suggests that remote (high latitude and altitude) Aucella Lake is highly sensitive and therefore a sentinel of climate change. The third phase recorded at Madsen Lake differs from the previous ones, representing more a reflection of regional climatic changes associated with the LIA onset (Catalan et al., 2013). The maximum glacial extent in the area occurred before ~0.5 cal. ka BP,

effectively during the beginning of the LIA, when an increase of nivation processes in Zackenberg Valley was recorded (Adamson et al., 2019), after which temperatures increased.

There have been several studies from the Aucella Lake region that have examined paleo-records from lacustrine and continental shelf sediments. Research has focused on areas to the north (Christiansen, 1998) and the south of our study area (Davies et al., 2022; Klug, 2009; Pados-Dibattista et al., 2022; Schmidt et al., 2011; Wagner et al., 2008b). Records from these two regions broadly agree with the structure of a cold Early Holocene, a warmer Mid-Holocene with a Holocene Thermal Maximum ending at ~5.5 cal. ka BP, and a relatively cold Late Holocene (Axford et al., 2017; Cremer et al., 2001a, 2001b; Klug and Wagner, 2008; Kolling et al., 2017; Levy et al., 2014a; Lowell et al., 2013; Lusas et al., 2017; Medford et al., 2021; Wagner et al., 2000, 2005; Wagner and Melles, 2002). Around 6.2 cal. ka BP, sub-surface waters on the Central Northeast Greenland shelf started to cool (Klug, 2009). After ~5.5 cal. ka BP a distinct cooling commenced with an increase in sea ice-extents (Pados-Dibattista et al., 2022) showing a Neoglacial average cooling of 0.6–0.8 °C per thousand years from ~5.5 to ~0.5 cal. ka BP that was more intense between ~4 to ~3.5 cal. ka BP and became progressively colder throughout the late Holocene (4.2 cal. ka BP-present) (Klug, 2009; Klug and Wagner, 2008). In some cases, the records also show greater productivity in the early and middle Holocene than in the late Holocene (Axford et al., 2017; Pados-Dibattista et al., 2022). Across the entire set of records, there is no strong consensus on the timing of the Neoglacial or other events such as the LIA. The closest to our study area was reported as the onset of the Neoglaciation at ~3.2–3.5 cal. ka BP glacial advance was reported as the onset of the Neoglaciation (Lusas et al., 2017) accompanied by a reconstructed negative temperature anomaly (Medford et al., 2021) and a cooling of the sub-surface water on the central Northeast Greenland shelf at 3.2 cal. ka BP (Axford et al., 2017). A shift towards more arid conditions at was recorded ~2.7 cal. ka BP, when the atmospheric circulation over North Atlantic significantly changed (Pados-Dibattista et al., 2022), with the first signs of glacial regrowth at ~2.6 cal. ka BP (Wagner et al., 2008a) appearing initially in high-elevation interior locations. Diatom analyses suggested that some areas of NE Greenland were seasonally ice-free during much of the Holocene, with perennial ice cover developing only after 1.8 cal. ka BP (Cremer et al., 2001a, 2001b). A gradual change towards colder temperature conditions began after 1.8 cal. ka BP, as registered in other regions (Levy et al., 2014b). There is no consensus about the timing of the LIA, although most records have indicated cold events or glacial advances prior to or around ~700 cal. ka BP, including at ~1.3 cal. ka BP (Lusas et al., 2017) and ~1.0–0.8 cal. ka BP (Adamson et al., 2019; Medford et al., 2021), with a subsequent period of ice-marginal retreat at ~0.5 cal. ka BP (Adamson et al., 2019; Lusas et al., 2017; Medford et al., 2021).

5.3.1. Greenland correlations

We compared our XRF-inferred temperature first vector and the first diatom PCA axis with Greenland temperature records: the temperature reconstructions from the nearest coastal ice core, from Renland Ice Cap (Medford et al., 2021), and the high-resolution XRF-inferred temperature reconstruction from a SE Greenland lake (Vinther et al., 2008). Moreover, we compared our temperature change record to regional changes in summer and winter solar insolation at 65°N (Balascio et al., 2015).

There was spatial and temporal thermal heterogeneity between the different records. The Renland ice-core temperature record showed a general cooling trend for the 5000 years of data, which differed from the response of our diatom assemblages, possibly due to the different sensitivity of the proxies employed to reconstruct this lake process. Although Aucella Lake does not directly receive glacial meltwater and our data do not preserve a direct sedimentary record of glacier activity (advances and retreats), the climate variability inferred from its record mirrors local glacial oscillations. Six major Neoglacial advances (4.1, 3.9, 3.2, 2.8, 2.1, and 1.3 cal. ka BP) of the Kulusuk glaciers were inferred from the Kulusuk Lake sediment record study (Balascio et al., 2015); these were broadly consistent with those detected in Aucella Lake. The first Neoglacial advance coincided with the abrupt air temperature drop recorded in Aucella Lake, indicating that this event was not due to local factors but rather to regional forcing. This ice advance may have been caused by the progressively declining NH summer insolation and the timing of cooling episodes in the North Atlantic Ocean attributed to the increased strength of the East Greenland Current (Balascio et al., 2015). These advances are also reflected as cooling peaks in our temperature reconstruction from XRF PC1 and likely record local glacier advances during these periods.

The Aucella Lake data presents linkages with changes in winter (before ~0.8 cal. ka BP) and summer (after ~0.8 cal. ka BP) insolation (Fig. 4), with a shift during the Late Holocene into warmer conditions beginning shortly after the summer and winter insolation curves intersect (~1.2 cal. ka BP) (Berger and Loutre, 1991). When comparing our results with the general East Greenland Mean July temperature obtained from the average of several records using a compilation of pollen data from different sediment cores (Gajewski, 2015), the difference in temporal resolution becomes clear, as does the need for multiproxy studies in order to better understand lake system linkages to the environment and climate.

6. Conclusions

This study presents the first multi-proxy-high-resolution approach for the climate variability in this region for the last ~5000 years and shows that high altitude lakes act as sentinels and amplifiers of rapid high arctic changes, and that local, seasonally specific temperature reconstructions with high resolution multiproxy studies are needed for accurately characterizing climates of the past. Aucella Lake limnological conditions were determined by a mixture of local and regional factors, including the presence of a snow patch in the lake catchment and regional climate evolution. Water turbidity due to the input of fine terrigenous particles, as well as the duration and thickness of lake ice cover, play important roles in determining these limnological conditions. Our paleolimnological reconstruction reflected changes in summer climate. It highlighted the relatively warmer conditions of the mid-Holocene, and abrupt temperature decreases at the onset of the Late Holocene which coincided with the beginning of glacial advances elsewhere, and occurred when winter and summer insolation temperatures had a minimum difference in values. The temperature recovery started at ca. 2.8 cal. ka BP and peaked during the Medieval Climate Anomaly. However, this progressive temperature raise was punctuated by abrupt and short-lived cold periods such as that which marked the onset of the Roman Warm Period at ca. 2 cal. ka BP. The beginning of the Little Ice Age was characterized by marked decreases in air temperatures, reaching minimum values at the end of this period. The last 50 years of the Aucella Lake record were marked by abrupt temperature rises, the highest peaks of the last 5000 years and are reflective of current anthropogenic global warming.

Supplementary data to this article can be found online at https://doi.org/10.1016/j.scitotenv.2023.167713.

Declaration of competing interest

All authors have participated in (i) conception and design, or analysis and interpretation of the data; (ii) drafting the article or revising it critically for important intellectual content; and (iii) approval of the final version. This manuscript has not been submitted to, nor is under review at, another journal or other publishing venue.

Data availability

Data will be made available on request.

Acknowledgements

This research was funded by the project PALEOGREEN (CTM2017-87976-P) of the Spanish Ministry of Economy and Competitiveness. Field work was also supported by an INTERACT Transnational Access grant (Ref. 730938, GLACIGREEN) and by the Research Group ANTALP (Antarctic, Arctic, Alpine Environments; 2017-SGR-1102), funded by the Government of Catalonia. Julia Garcia-Oteyza was supported by an FPI fellowship from the Spanish Ministry of Science, Innovation and Universities.

CRediT authorship contribution statement

All the authors have been actively involved in the investigation presented in this work:

1. Julia **Garcia-Oteyza**. Writing of a first draft of the manuscript (text, table, and figures), analysis, data processing, laboratory tasks, discussion of the results.
2. Santiago **Giralt**. Coordination of the research and writing of a first draft of the manuscript, leading the fieldwork, laboratory analysis, sampling and data processing.
3. Sergi **Pla-Rabes**. Laboratory diatoms analysis, discussion of the results, contribution to the discussion and writing.
4. Dermot **Antoniades**. Writing of a first draft of the manuscript and subsequent text revisions, fieldwork, laboratory analysis, sampling and data processing.
5. Marc **Oliva**. Fieldwork. Interpretation and discussion of the results thorough correction of the manuscript.
6. Hamid **Ghanbari**. Laboratory processing of grain size and chrorophyll data results and contribution to the interpretation and revision of the manuscript.
7. Rodrigo **Osorio-Serrano**. Discussion of the results and contribution to the revision of the manuscript.
8. David **Palacios**. Fieldwork and discussion of the results and contribution to the revision of the manuscript.

References

Adamson, K., Lane, T., Carney, M., Bishop, T., Delaney, C., 2019. High-resolution proglacial lake records of pre-little ice age glacier advance, northeast Greenland. Boreas 48, 535–550. https://doi.org/10.1111/bor.12361.

Adrian, R., O'Reilly, C.M., Zagarese, H., Baines, S.B., Hesse, D.O., Keller, W., Livinstone, D.M., Sommaruga, R., Straile, D., Van Donk, E., Weyhenmeyer, G.A., Winder, M., 2009. Lakes as sentinels of climate change. Limnol. Oceanogr. 33, 2283–2297. https://doi.org/10.4319/lo.2009.54.6_part_2.2283.

Anderson, N., Saros, J.E., Bullard, J.E., Cahoon, S.M.P., McGowan, S., Bagshaw, E.A., Barry, C.D., Bindler, R., Burpee, B.T., Carrivick, J.L., Fowler, R.A., Fox, A.D., Fritz, S. C., Giles, M.E., Hamerlik, L., Ingeman-Nielsen, T., Law, A.C., Mernild, S.H., Northington, R.M., Osburn, C.L., Pla-Rabès, S., Post, E., Telling, J., Stroud, D.A., Whiteford, E.J., Yallop, M.L., Yde, A.J.C., 2017. The arctic in the twenty-first century: changing biogeochemical linkages across a paraglacial landscape of Greenland. Bioscience 67, 118–133. https://doi.org/10.1093/biosci/biw158.

Antoniades, D., Hamilton, P., Douglas, M., Smol, J., 2008. Diatoms of North America: the freshwater floras of Prince Patrick, Ellef Ringnes and northern Ellesmere Islands from the Canadian Arctic Archipelago. Iconogr. Diatomol. 17, 1–649.

Aschwanden, A., Fahnestock, M.A., Truffer, M., Brinkerhoff, D.J., Hock, R., Khroulev, C., Mottram, R., Abbas Khan, S., 2019. Contribution of the Greenland ice sheet to sea level over the next millennium. Sci. Adv. 5 https://doi.org/10.1126/sciadv.aav9396.

Axford, Y., Levy, L.B., Kelly, M.A., Francis, D.R., Hall, B.L., Langdon, P.G., Lowell, T.V., 2017. Timing and magnitude of early to middle Holocene warming in East Greenland inferred from chironomids. Boreas 46, 678–687. https://doi.org/10.1111/bor.12247.

Balascio, N.L., D'Andrea, W.J., Bradley, R.S., 2015. Glacier response to North Atlantic climate variability during the Holocene. Clim. Past 11, 1587–1598. https://doi.org/10.5194/cp-11-1587-2015.

Battarbee, R.W., Carvalho, L., Jones, V.J., Flower, et al., 2001. Diatom analysis. In: Smol, J.P., Birks, H.J.B. (Eds.), Tracking Environmental Change using Lake Sediments. Kluwer Academic Publishers, Last, Dordrecht, pp. 155–202.

Bennike, O., Sørensen, M., Fredskild, B., Jacobsen, B.H., BöCher, J., Amsinck, S.L., Jeppesen, E., Andreasen, C., Christiansen, H.H., Humlum, O., 2008. Late Quaternary environmental and cultural changes in the Wollaston Forland Region, Northeast Greenland. Adv. Ecol. Res. 40, 45–79. https://doi.org/10.1016/S0065-2504(07)00003-7.

Berger, A., Loutre, M.F., 1991. Insolation values for the climate of the last 10 million years. Quat. Sci. Rev. 10, 297–317. https://doi.org/10.1016/0277-3791(91)90033-Q.

Blaauw, Maarten, Andrés Christeny, J., 2011. Flexible paleoclimate age-depth models using an autoregressive gamma process. Bayesian Anal. 6 (3), 457–474.

Bonow, J.M., Japsen, P., 2021. Peneplains and tectonics in north-east greenland after opening of the North-East Atlantic. GEUS Bull. 45, 1–35. https://doi.org/10.34194/GEUSB.V45.5297.

Bouchard, G., Gajewski, K., Hamilton, P.B., 2004. Freshwater diatom biogeography in the Canadian Arctic archipelago. J. Biogeogr. 31, 1955–1973. https://doi.org/10.1111/j.1365-2699.2004.01143.x.

Briner, J.P., McKay, N.P., Axford, Y., Bennike, O., Bradley, R.S., de Vernal, A., Fisher, D., Francus, P., Fréchette, B., Gajewski, K., Jennings, A., Kaufman, D.S., Miller, G., Rouston, C., Wagner, B., 2016. Holocene climate change in Arctic Canada and Greenland. Quat. Sci. Rev. 147, 340–364. https://doi.org/10.1016/j.quascirev.2016.02.010.

Cable, S., Christiansen, H.H., Westergaard-Nielsen, A., Kroon, A., Elberling, B., 2018. Geomorphological and cryostratigraphical analyses of the Zackenberg Valley, NE Greenland and significance of Holocene alluvial fans. Geomorphology 303, 504–523.

Carpenter, S.R., Benson, B.J., Biggs, R., Chipman, J.W., Foley, J.A., Golding, S.A., Hammer, R.B., Hanson, P.C., Johnson, P.T.J., Kamarainen, A.M., Kratz, T.K., Lathrop, R.C., McMahon, K.D., Provencher, B., Rusak, J.A., Solomon, C.T., Stanley, E.H., Turner, M.G., Vander Zanden, M.J., Wu, C.H., Yuan, H., 2007. Understanding regional change: a comparison of two lake districts. Bioscience 57, 323–335. https://doi.org/10.1641/B570407.

Catalan, J., Pla-Rabés, S., Wolfe, A.P., Smol, J.P., Rühland, K.M., Anderson, N.J., Kopáček, J., Stuchlík, E., Schmidt, R., Koinig, K.A., Camarero, L., Flower, R.J., Heiri, O., Kamenik, C., Korhola, A., Leavitt, P.R., Psenner, R., Renberg, I., 2013. Global change revealed by palaeolimnological records from remote lakes: a review. J. Paleolimnol. 49, 513–535. https://doi.org/10.1007/s10933-013-9681-2.

CAVM Team, 2003. Circumpolar Arctic Vegetation Map. (1:7,500,000 scale), Conservation of Arctic Flora and Fauna (CAFF) Map No. 1. US Fish Wildl. Serv. AK. Available http://www.Geobot.uaf.edu/cavm/ [Verified 1 August 15 July 2015] 2.

Christiansen, H.H., 1998. "Little Ice Age" nivation activity in northeast Greenland. Holocene 8, 719–728. https://doi.org/10.1191/095968398666994797.

Christiansen, H.H., Sigsgaard, C., Humlum, O., Rasch, M., Hansen, B.U., 2008. Permafrost and periglacial geomorphology at Zackenberg. Adv. Ecol. Res. 40, 151–174. https://doi.org/10.1016/S0065-2504(07)00007-4.

Christiansen, H.H., Etzelmüller, B., Isaksen, K., Juliussen, H., Farbrot, H., Humlum, O., Johansson, M., Ingeman-Nielsen, T., Kristensen, L., Hjort, J., Holmlund, P., Sannel, A.B.K., Sigsgaard, C., Åkerman, H.J., Foged, N., Blikra, L.H., Pernosky, M.A., Ødegård, R.S., 2010. The thermal state of permafrost in the nordic area during the international polar year 2007-2009. Permafr. Periglac. Process. 21, 156–181. https://doi.org/10.1002/ppp.687.

Chung, 1974. Quantitative interpretation of X-ray diffraction patterns of mixtures: II. Adiabatic principles of X-ray diffraction analysis of mixtures. Structure 526–531.

Cremer, H., Melles, M., Wagner, B., 2001a. Holocene climate changes reflected in a diatom succession from Basaltsø, east Greenland. Can. J. Bot. 79, 649–656. https://doi.org/10.1139/cjb-79-6-649.

Cremer, H., Wagner, B., Melles, M., Hubberten, H.W., 2001b. The postglacial environmental development of Raffles Sø, East Greenland: inferences from a 10,000 year diatom record. J. Paleolimnol. 26, 67–87. https://doi.org/10.1023/A:1011179321529.

Davies, J., Mathiasen, A.M., Kristiansen, K., Hansen, K.E., Wacker, L., Alstrup, A.K.O., Munk, O.L., Pearce, C., Seidenkrantz, M.S., 2022. Linkages between ocean circulation and the Northeast Greenland Ice Stream in the Early Holocene. Quat. Sci. Rev. 286, 107530 https://doi.org/10.1016/j.quascirev.2022.107530.

Davini, P., Cagnazzo, C., Neale, R., Tribbia, J., 2012. Coupling between Greenland blocking and the North Atlantic Oscillation pattern. Geophys. Res. Lett. 39, 1–6. https://doi.org/10.1029/2012GL052315.

Docherty, C.L., Riis, T., Milner, A.M., Christofferson, K.S., Hannah, D.M., 2018. Controls on stream hydrochemistry dynamics in a high Arctic snow-covered watershed. Hydrol. Process. 32, 3327–3340. https://doi.org/10.1002/hyp.13256.

Emson, D., Sayer, C.D., Bennion, H., Patmore, I.R., Rioual, P., 2018. Mission possible: diatoms can be used to infer past duckweed (lemnoid Araceae) dominance in ponds. J. Paleolimnol. 60, 209–221. https://doi.org/10.1007/s10933-017-0008-6.

Fagel, N., Boës, X., 2008. Clay-mineral record in Lake Baikal sediments: the Holocene and Late Glacial transition. Palaeogeogr. Palaeoclimatol. Palaeoecol. 259, 230–243. https://doi.org/10.1016/j.palaeo.2007.10.009.

Finkelstein, S.A., Gajewski, K., 2008. Responses of Fragilarioid-dominated diatom assemblages in a small Arctic lake to Holocene climatic changes, Russell Island, Nunavut, Canada. J. Paleolimnol. 40, 1079–1095. https://doi.org/10.1007/s10933-008-9215-5.

Gajewski, K., 2015. Quantitative reconstruction of Holocene temperatures across the Canadian Arctic and Greenland. Glob. Planet. Chang. 128, 14–23. https://doi.org/10.1016/j.gloplacha.2015.02.003.

Garcia-Oteyza, J., Oliva, M., Palacios, D., Fernández-Fernández, J.M., Schimmelpfennig, I., Andrés, N., Antoniades, D., Christiansen, H.H., Humlum, O., Léanni, L., Jomelli, V., Ruiz-Fernández, J., Rinterknecht, V., Lane, T.P., Adamson, K., Aumaître, G., Bourlès, D., Keddadouche, K., 2022. Late Glacial deglaciation of the Zackenberg area, NE Greenland. Geomorphology 401, 108125.

Ghanbari, H., Antoniades, D., 2022. Convolutional neural networks for mapping of lake sediment core particle size using hyperspectral imaging. Int. J. Appl. Earth Obs. Geoinf. 112, 102906 https://doi.org/10.1016/j.jag.2022.102906.

Goosse, H., Kay, J.E., Armour, K.C., Bodas-Salcedo, A., Chepfer, H., Docquier, D., Jonko, A., Kushner, P.J., Lecomte, O., Massonnet, F., Park, H.S., Pithan, F., Svensson, G., Vancoppenolle, M., 2018. Quantifying climate feedbacks in polar regions. Nat. Commun. 9 https://doi.org/10.1038/s41467-018-04173-0.

Grimm, E.C., 1987. CONISS: a FORTRAN 77 program for stratigraphically constrained cluster analysis by the method of incremental sum of squares. Comput. Geosci. 13, 13–35. https://doi.org/10.1016/0098-3004(87)90022-7.

Hanna, E., Cropper, T.E., Jones, P.D., Scaife, A.A., Allan, R., 2015. Recent seasonal asymmetric changes in the NAO (a marked summer decline and increased winter variability) and associated changes in the AO and Greenland Blocking Index. Int. J. Climatol. 35, 2540–2554. https://doi.org/10.1002/joc.4157.

Hanna, E., Cropper, T.E., Hall, R.J., Cappelen, J., 2016. Greenland Blocking Index 1851–2015: a regional climate change signal. Int. J. Climatol. 36, 4847–4861. https://doi.org/10.1002/joc.4673.

Hasholt, B., Mernild, S.H., Sigsgaard, C., Elberling, B., Petersen, D., Jakobsen, B.H., Hansen, B.U., Hinkler, J., Søgaard, H., 2008. Hydrology and transport of sediment and solutes at Zackenberg. Adv. Ecol. Res. 40, 197–221. https://doi.org/10.1016/S0065-2504(07)00009-8.

Henriksen, N., Higgins, A.K., Kalsbeek, F., Pulvertaft, T.C.R., 2009. Greenland from Archaean to quaternary descriptive text to the 1995 geological map of Greenland, 1: 2500000. Geol. Surv. Denmark Greenl. Bull. 18, 126.

Hernández, A., Trigo, R.M., Pla-Rabes, S., Valero-Garcés, B.L., Jerez, S., Rico-Herrero, M., Vega, J.C., Jambrina-Enríquez, M., Giralt, S., 2015. Sensitivity of two Iberian lakes to North Atlantic atmospheric circulation modes. Clim. Dyn. 45, 3403–3417. https://doi.org/10.1007/s00382-015-2547-8.

Højlund Pedersen, S., 2017. Scaling-up Climate Change Effects in Greenland. PhD Thesis.. Aarhus University. Department of Bioscience, Denmark (178 pp).

Juggins, S., 2022. rioja: Analysis of Quaternary Science Data. R package version 1.0-5. https://cran.r-project.org/package=rioja.

Kassambara, A., Mundt, F., 2020. Factoextra: Extract and Visualize the Results of Multivariate Data Analyses. R Package Version 1.0.7. https://CRAN.Rproject.org/package=factoextra.

Klug, M., 2009. The late Quaternary environmental and climatic history of North-East Greenland, inferred from coastal lakes. PhD Thesis. Univ. Köln 148. https://doi.org/10.23689/fidgeo-241.

Klug, M., Wagner, B., 2008. Late Pleistocene and Holocene environmental history of northeastern Geographical Society Ø, East Greenland, inferred from Loon Lake s sediment record. Leipziger Geowissenschaften, Leipzig 1–22.

Kolling, H.M., Stein, R., Fahl, K., Perner, K., Moros, M., 2017. Short-term variability in late Holocene sea ice cover on the East Greenland Shelf and its driving mechanisms. Palaeogeogr. Palaeoclimatol. Palaeoecol. 485, 336–350. https://doi.org/10.1016/j.palaeo.2017.06.024.

Kottek, M., Grieser, J., Beck, C., Rudolf, B., Rubel, F., 2006. World map of the Köppen-Geiger climate classification updated. Meteorol. Z. 15, 259–263. https://doi.org/10.1127/0941-2948/2006/0130.

Krammer, K., Lange-Bertalot, H., 1986. 2/1. Bacillariophyceae. 1. Teil: Naviculaceae. In: Ettl, H., Gerloff, J., Heynig, H., Mollenhauer, D. (Eds.), Sübwasserflora von Mitteleuropa. G. Fischer Verlag, Stuttgart, Germany, 206 Tafeln mit 2976 Figuren. 876 pp.

Krammer, K., Lange-Bertalot, H., 1988. 2/2. Bacillariophyceae. 2. Teil: Bacillariaceae. Epithemiaceae, Surirellaceae. In: Ettl, H., Gerloff, J., Heynig, H., Mollenhauer, D. (Eds.), Sübwasserflora von Mitteleuropa. G. Fischer Verlag, Stuttgart, Germany, 184 Tafeln mit 1914 Figuren. 596 pp.

Krammer, K., Lange-Bertalot, H., 1991a. 2/3. Bacillariophyceae. 3. Teil: Centrales, Fragilariaceae, Eunotiaceae. In: Ettl, H., Gerloff, J., Heynig, H., Mollenhauer, D. (Eds.), Sübwasserflora von Mitteleuropa. G. Fischer Verlag, Stuttgart, 166 Tafeln mit 2180 Figuren. 576 pp.

Krammer, K., Lange-Bertalot, H., 1991b. 2/4. Bacillariophyceae. 4. Teil: Achnanthaceae. Kritische Ergänzungen zu Navicula (Lineolatae) und Gomphonema. In: Ettl, H., Gerloff, J., Heynig, H., Mollenhauer, D. (Eds.), Sübwasserflora von Mitteleuropa. G. Fischer Verlag, Stuttgart, 88 Tafeln mit 2048 Figuren. 437 pp.

Kuhn, D.L., Plafkin, J.L., Cairns, J., Lowe, R.L., 1981. Qualitative characterization of aquatic environments using diatom life-form strategies. Trans. Am. Microsc. Soc. 100, 165. https://doi.org/10.2307/3225800.

Legendre, P., Birks, H.J.B., 2012. Clustering and partitioning. Track. Environ. Chang. Lake Sediments 5, 1–32.

Legendre, P., Gallagher, E.D., 2001. Ecologically meaningful transformations for ordination of species data. Oecologia 129, 271–280. https://doi.org/10.1007/s004420100716.

Levy, L.B., Kelly, M.A., Lowell, T.V., Hall, B.L., Hempel, L.A., Honsaker, W.M., Lusas, A. R., Howley, J.A., Axford, Y.L., 2014a. Holocene fluctuations of Bregne ice cap, Scoresby Sund, east Greenland: a proxy for climate along the Greenland Ice Sheet margin. Quat. Sci. Rev. 92, 357–368. https://doi.org/10.1016/j.quascirev.2013.06.024.

Levy, L.B., Kelly, M.A., Lowell, T.V., Hall, B.L., Hempel, L.A., Honsaker, W.M., Lusas, A. R., Howley, J.A., Axford, Y.L., 2014b. Holocene fluctuations of Bregne ice cap, Scoresby Sund, east Greenland: a proxy for climate along the Greenland Ice Sheet margin. Quat. Sci. Rev. 92, 357–368. https://doi.org/10.1016/j.quascirev.2013.06.024.

Lowell, T.V., Hall, B.L., Kelly, M.A., Bennike, O., Lusas, A.R., Honsaker, W., Smith, C.A., Levy, L.B., Travis, S., Denton, G.H., 2013. Late Holocene expansion of Istorvet ice cap, Liverpool Land, east Greenland. Quat. Sci. Rev. 63, 128–140. https://doi.org/10.1016/j.quascirev.2012.11.012.

Lund, M., Abermann, J., Skov, K., 2017. Environmental effects of a rare rain event in the high Arctic. In: EGUGeneralAssembly Conf. Abstr. 1 19, Abstract no. 9462.

Lusas, A.R., Hall, B.L., Lowell, T.V., Kelly, M.A., Bennike, O., Levy, L.B., Honsaker, W., 2017. Holocene climate and environmental history of East Greenland inferred from lake sediments. J. Paleolimnol. 57, 321–341. https://doi.org/10.1007/s10933-017-9951-5.

McFarlin, J.M., Axford, Y., Osburn, M.R., Kelly, M.A., Osterberg, E.C., Farnsworth, L.B., 2018. Pronounced summer warming in northwest Greenland during the Holocene and Last Interglacial. Proc. Natl. Acad. Sci. U. S. A. 115 (25), 6357–6362.

Medford, A.K., Hall, B.L., Lowell, T.V., Kelly, M.A., Levy, L.B., Wilcox, P.S., Axford, Y., 2021. Holocene glacial history of Renland Ice Cap, East Greenland, reconstructed from lake sediments. Quat. Sci. Rev. 258, 106883 https://doi.org/10.1016/j.quascirev.2021.106883.

Miller, G.H., Alley, R.B., Brigham-Grette, J., Fitzpatrick, J.J., Polyak, L., Serreze, M.C., White, J.W.C., 2010. Arctic amplification: can the past constrain the future? Quat. Sci. Rev. 29, 1779–1790. https://doi.org/10.1016/j.quascirev.2010.02.008.

Oksanen, J.; Blanchet, F.G.; Friendly, M.; Kindt, R.; Legendre, P.; McGlinn, D.; Minchin, P.; O'Hara, R.B.; Simpson, G.; Solymos, P.; Stevens, M.H.H.; Szöcs, E.; Wagner, H., 2020. vegan community ecology package. version 2.5-7.

Oerlemans, J., 2001. Climatic interpretation of glacier fluctuations. In: Oerlemans, J. (Ed.), Glaciers and Climate Change. A.A. Balkema Publishers, Lisse, Netherlands, pp. 93–107.

Pados-Dibattista, T., Pearce, C., Detlef, H., Bendtsen, J., Seidenkrantz, M.S., 2022. Holocene palaeoceanography of the Northeast Greenland shelf. Clim. Past 18, 103–127. https://doi.org/10.5194/cp-18-103-2022.

Paull, T.M., Hamilton, P.B., Gajewski, K., LeBlanc, M., 2008. Numerical analysis of small Arctic diatoms (Bacillariophyceae) representing the *Staurosira* and *Staurosirella* species complexes. Phycologia 47, 213–224. https://doi.org/10.2216/07-17.1.

Pham, S.V., Leavitt, P.R., McGowan, S., Peres-Neto, P., 2008. Spatial variability of climate and land-use effects on lakes of the northern Great Plains. Limnol. Oceanogr. 53, 728–742. https://doi.org/10.4319/lo.2008.53.2.0728.

Pithan, F., Mauritsen, T., 2014. Arctic amplification dominated by temperature feedbacks in contemporary climate models. Nat. Geosci. 7, 181–184. https://doi.org/10.1038/ngeo2071.

Post, E., Forchhammer, M.C., Bret-Harte, M.S., Callaghan, T.V., Christensen, T.R., Elberling, B., Fox, A.D., Gilg, O., Hik, D.S., Høye, T.T., Ims, R.A., Jeppesen, E., Klein, D.R., Madsen, J., McGuire, A.D., Rysgaard, S., Schindler, D.E., Stirling, I., Tamstorf, M.P., Tyler, N.J.C., Van Der Wal, R., Welker, J., Wookey, P.A., Schmidt, N. M., Aastrup, P., 2009. Ecological dynamics across the Arctic associated with recent climate change. Science 325, 1355–1358. https://doi.org/10.1126/science.1173113.

Preusser, F., Degering, D., Fuchs, M., Hilgers, A., Kadereit, A., Klasen, N., Krbetschek, M., Richter, D., Spencer, J.Q.G., 2008. Luminescence dating: basics, methods and applications. Quat. Sci. J. 57, 95–149. https://doi.org/10.3285/eg.57.1-2.5.

R Core Team, 2022. R: A Language and Environment for Statistical Computing. R Foundation for Statistical Computing, Vienna, Austria. URL. https://www.R-project.org/.

Reimer, P.J., Austin, W.E.N., Bard, E., Bayliss, A., Blackwell, P.G., Ramsey, C.B., Butzin, M., Cheng, H., Edwards, R.L., Friedrich, M., Grootes, P.M., Guilderson, T.P., Hajdas, I., Heaton, T.J., Hogg, A.G., Hughen, K.A., Kromer, B., Manning, S.W., Muscheler, R., Palmer, J.G., Pearson, C., van der Plicht, J., Reimer, R.W., Richards, D.A., Scott, E.M., Southon, J.R., Turney, C.S.M., Wacker, L., Adolphi, F., Büntgen, U., Capano, M., Fahrni, S.M., Fogtmann-Schulz, A., Friedrich, R., Köhler, P., Kudsk, S., Miyake, F., Olsen, J., Reinig, F., Sakamoto, M., Sookdeo, A., Talamo, S., 2020. The IntCal20 Northern Hemisphere radiocarbon age calibration curve (0–55 Cal KBP). Radiocarbon 62 (4), 725–757.

Rosenzweig, C., 2007. Assessment of observed changes and responses in natural and managed systems. In: Parry, M.L., Canz, O.F., Palutikof, J.P., van der Linden, P.J., Hanson, C.E. (Eds.), Clim. Chang. 2007—Impacts, Adapt. Vulnerability. Contrib. Work. Gr. II to Fourth Assess. Rep. Intergov. Panel 79–131.

Sánchez-López, G., Hernández, A., Pla-Rabes, S., Toro, M., Granados, I., Sigró, J., Trigo, R.M., Rubio-Inglés, M.J., Camarero, L., Valero-Garcés, B., Giralt, S., 2015. The effects of the NAO on the ice phenology of Spanish alpine lakes. Clim. Chang. 130, 101–113. https://doi.org/10.1007/s10584-015-1353-y.

Saros, J.E., Anderson, N.J., Juggins, S., McGowan, S., Yde, J.C., Telling, J., Bullard, J.E., Yallop, M.L., Heathcote, A.J., Burpee, B.T., Fowler, R.A., Barry, C.D., Northington, R. M., Osburn, C.L., Pla-Rabes, S., Mernild, S.H., Whiteford, E.J., Grace Andrews, M., Kerby, J.T., Post, E., 2019. Arctic climate shifts drive rapid ecosystem responses across the West Greenland landscape. Environ. Res. Lett. 14 https://doi.org/10.1088/1748-9326/ab2928.

Schmidt, S., Wagner, B., Heiri, O., Klug, M., Bennike, O., Melles, M., 2011. Chironomids as indicators of the Holocene climatic and environmental history of two lakes in Northeast Greenland. Boreas 40, 116–130. https://doi.org/10.1111/j.1502-3885.2010.00173.x.

Serreze, M.C., Barry, R.G., 2011. Processes and impacts of Arctic amplification: a research synthesis. Glob. Planet. Chang. 77, 85–96. https://doi.org/10.1016/j.gloplacha.2011.03.004.

Smol, J.P., 1983. Paleophycology of a high arctic lake near Cape Herschel, Ellesmere Island. Can. J. Bot. 61, 2195–2204. https://doi.org/10.1139/b83-238.

St-Onge, G., Mulder, T., Francus, P., Long, B., 2007. Chapter two continuous physical properties of cored marine sediments. Dev. Mar. Geol. 1, 63–98. https://doi.org/10.1016/S1572-5480(07)01007-X.

Tomkins, J.D., Antoniades, D., Lamoureux, S.F., Vincent, W.F., 2008. A simple and effective method for preserving the sediment-water interface of sediment cores during transport. J. Paleolimnol. 40, 577–582. https://doi.org/10.1007/s10933-007-9175-1.

Vinther, B.M., Clausen, H.B., Fisher, D.A., Koerner, R.M., Johnsen, S.J., Andersen, K.K., Dahl-Jensen, D., Rasmussen, S.O., Steffensen, J.P., Svensson, A.M., 2008.

Synchronizing ice cores from the Renland and Agassiz ice caps to the Greenland Ice Core Chronology. J. Geophys. Res. Atmos. 113, 1–10. https://doi.org/10.1029/2007JD009143.

Wagner, B., Melles, M., 2002. Holocene environmental history of western Ymer, East Greenland, inferred from lake sediments. Quat. Int. 89, 165–176. https://doi.org/10.1016/S1040-6182(01)00087-8.

Wagner, B., Melles, M., Hahne, J., Niessen, F., Hubberten, H.W., 2000. Holocene climate history of Geographical Society φ, East Greenland - evidence from lake sediments. Palaeogeogr. Palaeoclimatol. Palaeoecol. 160, 45–68. https://doi.org/10.1016/S0031-0182(00)00046-8.

Wagner, B., Heiri, O., Hoyer, D., 2005. Chironomids as proxies for palaeoenvironmental changes in East Greenland: a Holocene record from Geographical Society Ø. Zeitschrift der Dtsch. Gesellschaft für Geowissenschaften 156, 543–556. https://doi.org/10.1127/1860-1804/2005/0156-0543.

Wagner, B., Bennike, O., Bos, J.A.A., Cremer, H., Lotter, A.F., Melles, M., 2008a. A multidisciplinary study of Holocene sediment records from Hjort Sø on Store Koldewey, Northeast Greenland. J. Paleolimnol. 39, 381–398. https://doi.org/10.1007/s10933-007-9120-3.

Wagner, B., Bennike, O., Bos, J.A.A., Cremer, H., Lotter, A.F., Melles, M., 2008b. A multidisciplinary study of Holocene sediment records from Hjort Sø on Store Koldewey, Northeast Greenland. J. Paleolimnol. 39, 381–398. https://doi.org/10.1007/s10933-007-9120-3.

Williamson, C.E., Dodds, W., Kratz, T.K., Palmer, M.A., 2008. Lakes and streams as sentinels of environmental change in terrestrial and atmospheric processes. Front. Ecol. Environ. 6, 247–254. https://doi.org/10.1890/070140.

Williamson, C.E., Saros, J.E., Schindler, D.W., 2009. Climate change: sentinels of change. Science 323, 887–888. https://doi.org/10.1126/science.1169443.